SUPPORTING INFORMATION

Adhesion of fluid infused silicone elastomer to glass

Anushka Jha[1], Preetika Karnal[1,2], and Joelle Frechette[1,3,*]

1. Chemical and Biomolecular Engineering Department, Johns Hopkins University, Baltimore, MD 21218, USA 2. Department of Chemical and Biomolecular Engineering, Lehigh University, 124 E Morton St, Building 205, Bethlehem, Pennsylvania 18015, United States 3. Chemical and Biomolecular Engineering Department, University of California, Berkeley, CA 94760, USA

Table of Contents

1. Sample preparation

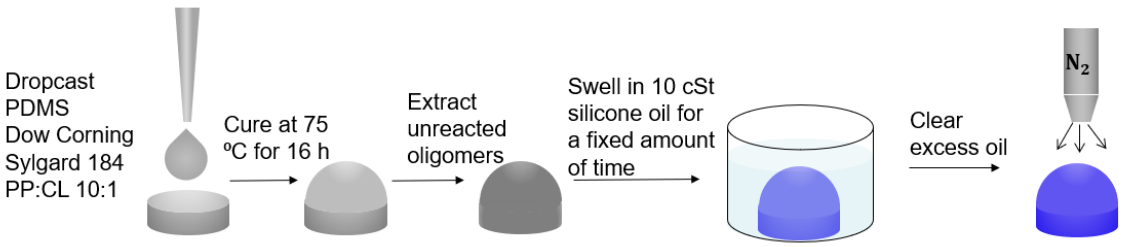

Fig. S1. Schematic for dropcasting[1], cure and swelling of PDMS (Sylgard 184).

2. Swelling dynamics of PDMS probe

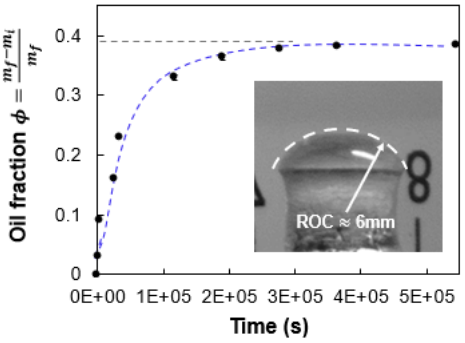

Fig. S2. Mass swelling of 10:1 PDMS in 10 cSt silicone oil after hexane extraction.

3. Rheology of dry and swollen PDMS

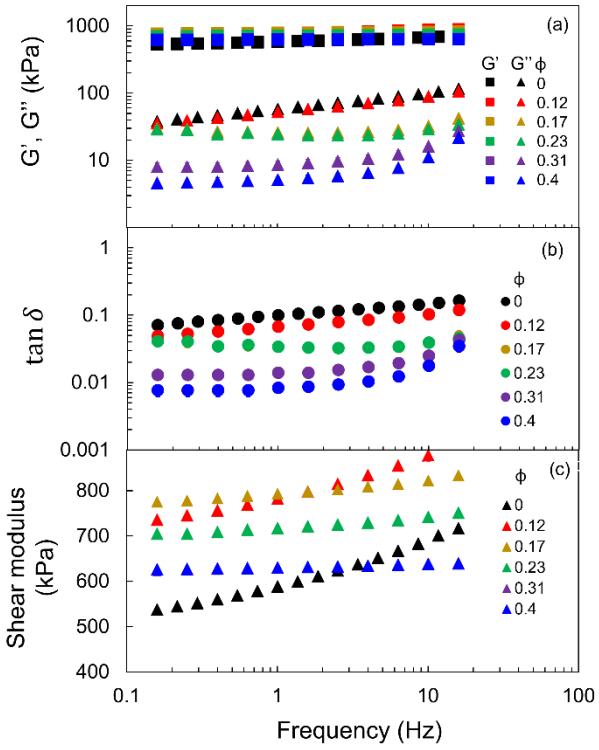

Fig. S3. Rheological properties as a function of oil mass fraction of swollen PDMS. (a) Storage modulus (G', squares) and Loss modulus (G'', triangles) (b) $\tan\delta$ = G''/G' (c) Shear modulus $G = \sqrt{G'^2 + G''^2}$ as a function of frequency ($f\ (Hz) = \omega(rad/s)/2\pi$) at different oil fractions.

According to the theory of rubber elasticity (**Eq. S1**), the shear modulus should decrease with increasing oil fraction. This expected decrease is due to reduction in the mass density of crosslinks ρ/M_C as the volume of the elastomer expands as given by:

$$G = \frac{\rho RT}{M_c}. \tag{S1}$$

Here G is the shear modulus of the swollen elastomer calculated from oscillatory rheology (**Fig. S3c**), ρ is the mass density of the elastomer and M_C is the number-average molecular weight of the chain between crosslinks. Instead of a decrease we observe a slight increase in shear modulus from $\phi = 0$ to $\phi = 0.1$, followed by a subsequent decrease with increasing oil fraction. We suspect that the initial deviation from ideal rubber-like behavior is due to the presence of silica fillers in the Sylgard elastomer kit. Upon extraction, some of these silica particles may be removed from the system leaving behind voids that are filled by silicone oil upon initial swelling, without increasing the volume of the swollen sample. Subsequently, as the amount of oil in the bulk increases from $\phi = 0.1$ to $\phi = 0.4$, the overall volume of the elastomer also increases. This results in decreasing density of crosslinks and therefore, decrease in the shear modulus.

4. Connecting swelling and rheology data

The volume swelling ratio, Λ_{swell} way can be compared to the equilibrium oil fraction from Flory-Rehner theory.[2, 3] According to Flory-Rehner theory, at equilibrium swelling, the volume fraction of oil Λ_{F-R} in the can be expressed using **Eq. (S2)**

$$ln(\Lambda_{F-R}) + (1 - \Lambda_{F-R}) + \chi(1 - \Lambda_{F-R})^2 + \frac{\rho_e V_s}{M_c}(1 - \Lambda_{F-R})^{1/3} = 0 \tag{S2}$$

Where χ is the Flory Huggins interaction parameter, V_s is the molar volume of the oil. ρ_e is the mass density of the elastomer at maximum swelling and M_C can be obtained from theory of rubber elasticity given in Eq. (S1). Assuming that $\chi \approx 0$ for a chemical similar combination of PDMS elastomer and silicone oil, we obtain $\Lambda_{F-R} = 0.42$ which is similar to the volume oil fraction Λ_{swell} obtained from swelling measurements.

5. Choice of frequency for comparison

For a rate of debonding of $v_{deb} = 50$ μm/s, and displacement during detachment: δ~ 30-70 μm, we can calculate an effective strain rate (extensional) as $\frac{\delta}{v} \sim 0.6 - 1.4$ Hz, which is similar to the chosen rheological frequency (1 Hz). We recognize that the two values may not be identical due to the different geometry of the experiments but this appears to be a good first approximation.

6. Rate dependence of G_C

We assume similar rate dependence for G_C based on the empirical relationship given as[4] $G_C = w\left(1 + \Phi(a_T v)\right)$ where w is the thermodynamic work of adhesion and ϕ is a dimensionless number that depends on the viscoelastic properties of the material and crack speed v. It has been seen that $w\left(\Phi(a_T v)\right) \propto G'(\omega)h$ [5] where G' is the storage modulus of the system and h is the sample thickness. It can be seen from the plot of G'vs ϕ (**Fig S3a**) that G' is similar across samples at different oil fractions. Additionally, we do not see any change in the slope of the $F - \delta$ curve which indicates similar mechanical properties at the given debonding velocity.

7. Moduli from PRI

Table S1. Values of effective Young's moduli calculated via **Eq. (4)**.

ϕ	E_0^*	E_V^*	E_P^*
			MPa
0	3.6 ± 0.4	3.0 ± 0.4	--
0.1	2.8 ± 0.3	2.7 ± 0.3	2.5 ± 0.3
0.4	3.0 ± 0.5	2.9 ± 0.5	2.3 ± 0.7
0.4 (in oil)	2.6 ± 0.5	2.5 ± 0.4	2.3 ± 0 .4

8. Mesh size calculation

Mesh size was calculated by using the following two equations:[6]

$$G = \frac{NkT}{\lambda_0} \qquad \text{(Rubber elasticity)}$$

$$\frac{4}{3}\pi\left(\frac{\xi}{2}\right)^3 = \frac{N}{\lambda_0^3} \qquad \text{(Chan et al, 2012, Ref 31, main text)}$$

Symbol	Description	Value
G	Shear Modulus at swelling equilibrium	630244 ± 67192 Pa
N	Number density of crosslinks	$\mathrm{mol/m^3}$
k	Boltzmann constant	1.38×10^{-23} J/K
T	Temperature	298.15 K
λ_0	Equilibrium swelling ratio $= \left(\frac{V_0}{V_i}\right)^{1/3}$	1.21 ± 0.01
ξ	Mesh size	2.6 nm

9. Surface energy determination

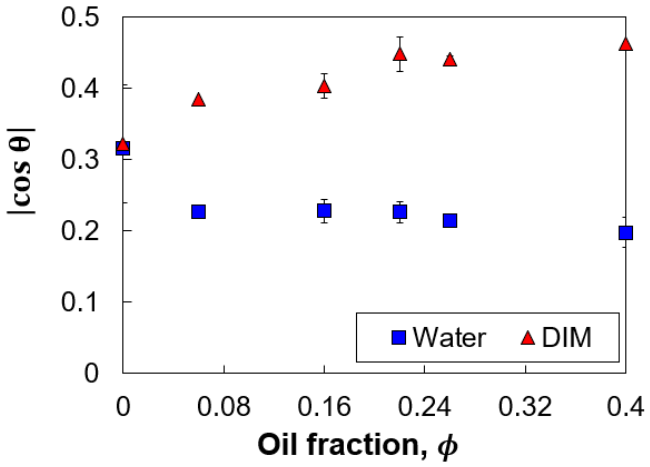

Fig. S4. Absolute value of cosine of contact angle, $|cos\ \theta|$ for water (blue squares) and diiodomethane (DIM) (red triangles) on swollen PDMS at different oil fraction. (Numerical values in **Table S3**).

Table S2. Values of dispersive(γ_d) and polar(γ_p) contributions to surface energy (γ) of water and DIM[7] used to obtain surface energy (SFE) of swollen PDMS using the two liquid method (OWRK)[8], **Eq. S3.**

	γ	γ_p (mJ/m^2)	γ_d	**Dominant component of SFE**
Water (w)	72	50.4	21.6	Polar
DIM (dim)	50	2.3	47.7	Dispersive

$$(1+\cos\theta_w)\left(\gamma_w^d+\gamma_w^p\right)=2\left(\sqrt{\gamma_w^d\gamma_s^d}+\sqrt{\gamma_w^p\gamma_s^p}\right)$$
$$(1+\cos\theta_{dim})\left(\gamma_{dim}^d+\gamma_{dim}^p\right)=2\left(\sqrt{\gamma_{dim}^d\gamma_s^d}+\sqrt{\gamma_{dim}^p\gamma_s^p}\right) \quad \text{(S3)}$$

Table S3. Calculation of surface of swollen elastomers from the two-liquid method (OWRK)[7, 8] as a function of oil fractions using **Eq. (S3).**

ϕ	Contact angle (°)		$\cos\theta$		γ_S (mJ/m^2)
	DIM	**Water**	**DIM**	**Water**	
0	71.2 ± 5.0	108.4 ± 0.4	0.32 ± 0.08	-0.32 ± 0.01	16.2 ± 1.9
0.06	67.4 ± 0.0	103.2 ± 0.0	0.38 ± 0.00	-0.23 ± 0.00	18.8 ± 0.0

0.16	66.3 ± 1.1	103.2 ± 1.0	0.40 ± 0.02	-0.23 ± 0.02	19.0 ± 0.5
0.22	63.4 ± 1.5	103.1 ± 0.8	0.45 ± 0.02	-0.23 ± 0.01	19.8 ± 0.6
0.26	63.8 ± 0.3	102.4 ± 0.6	0.44 ± 0.00	-0.21 ± 0.01	19.9 ± 0.2
0.4	62.4 ± 0.0	101.4 ± 1.3	0.46 ± 0.00	-0.20 ± 0.02	20.7 ± 0.3

10. Protocol for adhesion measurements

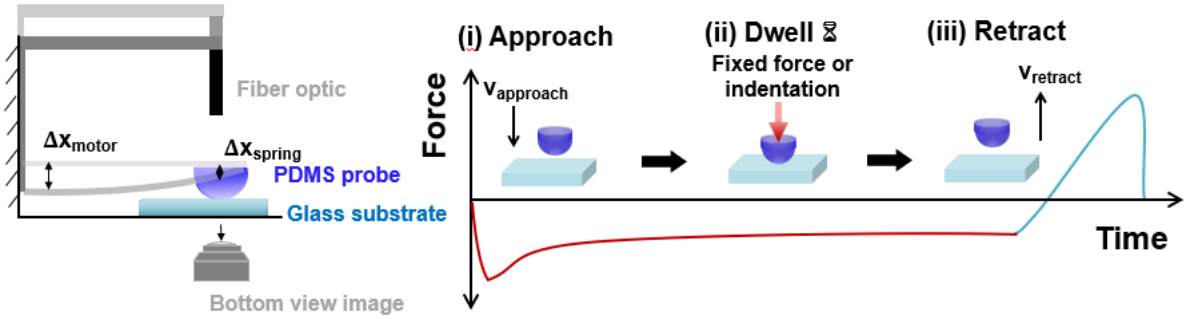

Fig. S5. Schematic for PRI and probe tack experiments.

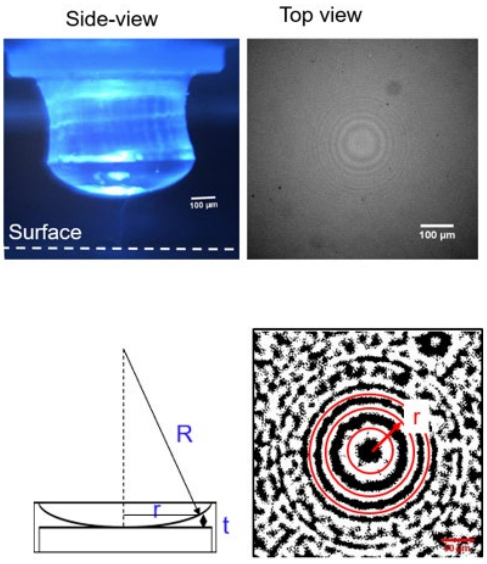

Fig. S6. Setting the 'zero' position using side/bottom view imaging.

Table S4. Calculation of gap when the lens is in "zero position" and comparison with predictions from thin film interference of visible light.

Bright ring #	r (μm)	$t=r^2/2R$ (nm)	$t= (2m+1)\ \lambda/4$ (nm)	
			λ=400 nm	λ=700 nm
1	33.5	102	100	175
2	66.4	400	300	525
3	89.2	724	500	875
4	108.7	1075	700	1225

11. Formation of capillary bridge during debonding of swollen PDMS

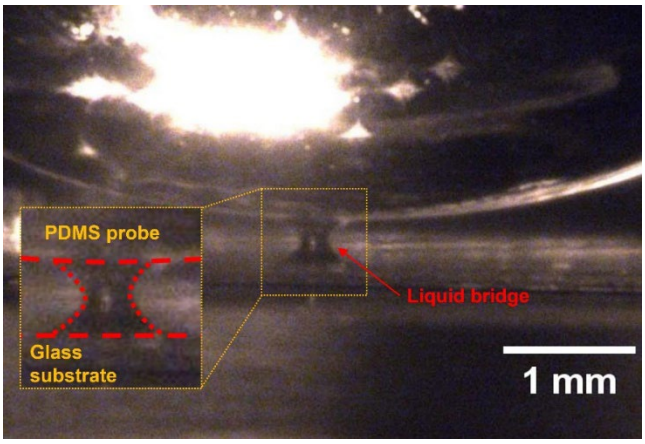

Fig. S7. Liquid capillary bridge seen during debonding of fully swollen PDMS from glass.

12. Model for adhesion model that combines capillary and contact forces.

During debonding, the total force acting on the probe, F_{tot} can be assumed to be a sum of the capillary F_{cap} and solid-solid contact force F_{JKR}:

$$F_{tot} = F_{cap} + F_{JKR}. \quad \text{(S4)}$$

Before the PDMS probe jumps out of contact (**Fig. S8a**), the contribution of capillary force and JKR adhesion to the total force can be given by:

$$F_{cap} = -4\pi\gamma_{oil}R, \quad \text{(S5)}$$

$$F_{JKR} = \frac{4}{3}E^*a^3 - 2\sqrt{2\pi w_{adh}E^*a^3}, \quad \text{(S6a)}$$

$$\delta = \frac{a^2}{R} - \sqrt{\frac{2\pi w_{adh}a}{E^*}}, \quad \text{(S6b)}$$

where $\gamma_{oil} = 20\, mJ/m^2$ is the surface tension of oil, R is the radius of curvature of the probe, $E^* \approx 2MPa$ is the effective Young's modulus of the material obtained from rheology, and a is contact radius calculated from **Eq. S6b**. (We cannot image the actual solid-solid contact area due to the presence of the oil meniscus.) The work of adhesion w_{adh} in Eq. S7 is calculated by assuming a simple mixing rule given in Eq. S8[9]:

$$\mathrm{w}_{adh} = \gamma_{\mathrm{PDMS,\,air}} + \gamma_{\mathrm{glass,\,air}} - \gamma_{\mathrm{PDMS,\,glass}}, \tag{S7}$$

$$w_{adh} \approx 2\sqrt{\gamma_{PDMS,air}\,\gamma_{glass,air}}. \tag{S8}$$

Since, $w_{PDMS} \approx 20$ mJ/m^2 and $w_{glass} \approx 65$ mJ/m^2 for pirahna cleaned glass slides, we get $w_{adh} \approx 72$ mJ/m^2. Solid-solid contact would undergo contact aging with time which is incorporated into our model by varying the work of adhesion using the equation for contact aging:

$$w_{adh}(t) = w_{adh,ref}\left(t/t_{ref}\right)^{n}, \tag{S9}$$

and $w_{adh,ref} = 72\ mJ/m^2$ and $t_{ref} = 100\, s$ (for simplicity). We assume that dry contact (if any) ages similarly in time as the dry PDMS and use $n = 0.042$ as the power law exponent to obtain an estimate for aging of solid-solid contact. Using $w_{adh}(t)$, we estimate the force as a function of contact time using **Eq. S6a,b** and plotted in **Fig. S9**.

The total force prior to detachment is a sum of the right hand side of **Eq. S5** and **Eq. S6a.** The initial slope of the force-time curve (**Fig. S8c**) is due to the elasticity of the lens contributing to the net compliance of the lens-cantilever system.

After the probe detaches (**Fig. S8b**), the contribution from JKR adhesion vanishes ($F_{JKR} = 0$). The only contribution to the total force is from the capillary bridge[10]:

$$\mathrm{F_{cap}} = -\frac{4\pi\gamma_{\mathrm{oil}}\mathrm{R}\cos\theta}{1 + \mathrm{H}/\mathrm{d}_{\frac{\mathrm{sp}}{\mathrm{pl}}}} - 2\pi\gamma_{\mathrm{oil}}\mathrm{R}\sin(\theta + \alpha), \tag{S10}$$

Here θ is the contact angle of oil on glass ≈ 0°, α: embracing angle, H is the height of liquid bridge at the center, $\mathrm{d}_{\frac{\mathrm{sp}}{\mathrm{pl}}}$ is the difference between the height of the liquid bridge at the periphery and at the center H. Using an estimate for the volume of the liquid bridge, V, we can calculate both $d_{\frac{sp}{pl}}$ and α:

$$d_{\frac{sp}{pl}} = -H + \sqrt{H^2 + \frac{V}{\pi R}} = \frac{R\alpha^2}{2}. \quad \text{(S11)}$$

By fitting the tail of the force time curve (after detachment), we obtain an estimate for the volume of the liquid bridge $\sim 0.01\mu L$. We know the values for γ_{oil}, R, θ and obtain a theoretical estimate for the capillary force. We see that the liquid meniscus contributes significantly to the overall force, even with the presence of some solid-solid adhesion at the interface (different lines in **Fig. 8c**).

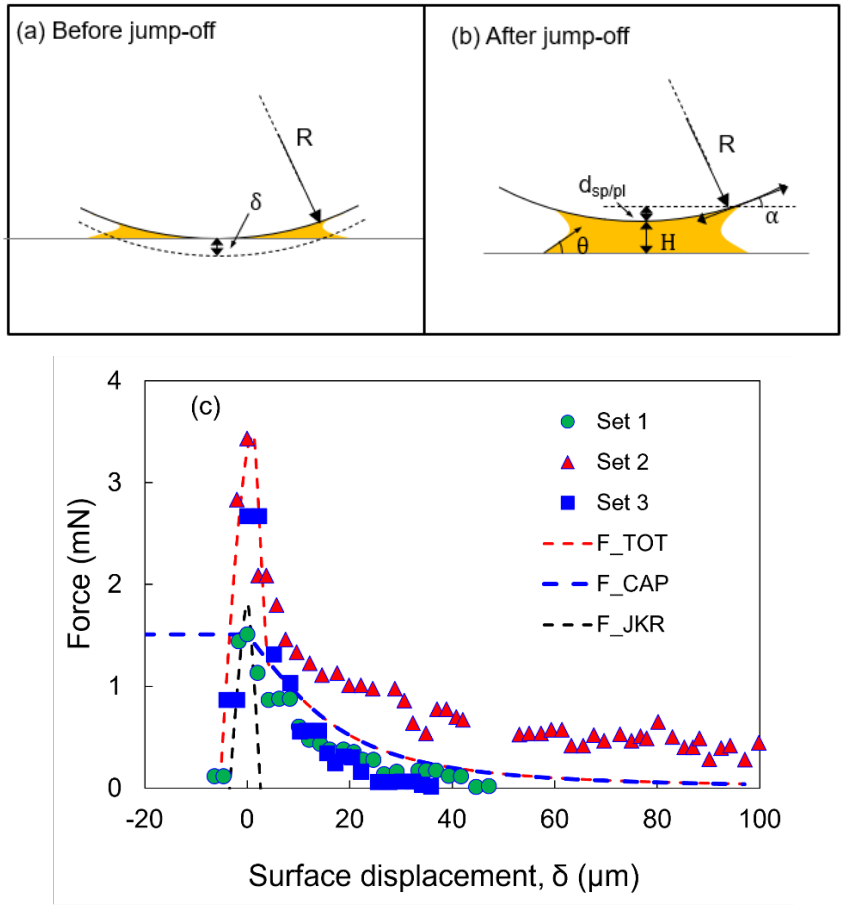

Fig. S8. Side view schematic of liquid bridge contact between fully swollen PDMS (sphere) and glass (flat) (a) Before jump off (b) After jump-off (c) Comparing results from probe-tack with capillary/JKR adhesion model (contact time=100s, $w_{adh} = 72\ mJ/m^2$).

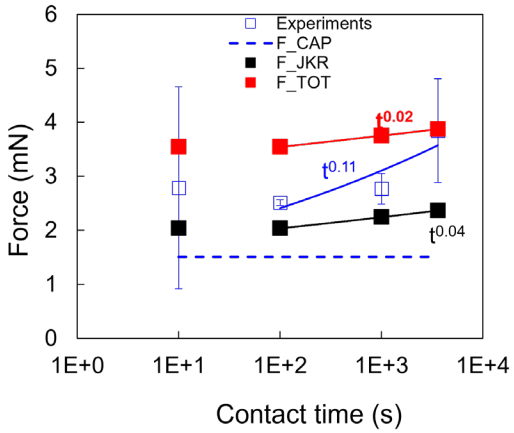

Fig. S9. Comparing capillary, JKR pull-off and total pull-off force for different contact times during detachment of fully swollen probe from glass after PRI experiments. Red, blue and black lines represent power law dependence of pull-off force on time.

References

1. S. Ekgasit, N. Kaewmanee, P. Jangtawee, C. Thammacharoen and M. Donphoongpri, Elastomeric PDMS Planoconvex Lenses Fabricated by a Confined Sessile Drop Technique, *ACS Appl. Mater. Interfaces*, 2016, **8**, 20474-20482.
2. P. J. Flory, Statistical Mechanics of Swelling of Network Structures, *J. Chem. Phys.*, 1950, **18**, 108-111.
3. P. J. Flory and J. Rehner, Statistical mechanics of cross-linked polymer networks II Swelling, *J. Chem. Phys.*, 1943, **11**, 521-526.
4. D. Maugis and M. Barquins, Fracture mechanics and the adherence of viscoelastic bodies, *J. Phys. D: Appl. Phys.*, 1978, **11**, 1989-2023.
5. C. Creton and M. Ciccotti, Fracture and adhesion of soft materials: a review, *Reports on Progress in Physics*, 2016, **79**, 046601.
6. Y. H. Hu, X. Chen, G. M. Whitesides, J. J. Vlassak and Z. G. Suo, Indentation of polydimethylsiloxane submerged in organic solvents, *J. Mater. Res.*, 2011, **26**, 785-795.
7. K. Efimenko, W. E. Wallace and J. Genzer, Surface Modification of Sylgard-184 Poly(dimethyl siloxane) Networks by Ultraviolet and Ultraviolet/Ozone Treatment, *J. Colloid Interface Sci.*, 2002, **254**, 306-315.
8. D. K. Owens and R. C. Wendt, Estimation of Surface Free Energy of Polymers, *J. Appl. Polym. Sci.*, 1969, **13**, 1741-&.
9. J. N. Israelachvili, in *Intermolecular and Surface Forces (Third Edition)*, ed. J. N. Israelachvili, Academic Press, Boston, 2011, DOI: https://doi.org/10.1016/B978-0-12-391927-4.10017-9, pp. 415-467.
10. Y. I. Rabinovich, M. S. Esayanur and B. M. Moudgil, Capillary forces between two spheres with a fixed volume liquid bridge: Theory and experiment, *Langmuir*, 2005, **21**, 10992-10997.